Haze Detection and Removal in High Resolution Satellite Image with Wavelet Analysis

Yong Du[1], Bert Guindon[2] and Josef Cihlar[2]

1) Intermap Technologies Inc., Ottawa, ON, K2E 1A2

2) Canada Centre for Remote Sensing, Ottawa, ON, K1A 0Y7

Submitted to:

IEEE Transactions on Geoscience and Remote Sensing

Corresponding author:

Yong DU (PhD)
Room 403, 588 Booth Street
Ottawa, ON
Canada K1A 0Y7
Yong.du@ccrs.nrcan.gc.ca

Abstract

A procedure for haze detection and removal from high-resolution satellite image using wavelet analysis (HAWAT) has been developed. It involves the analysis of the low spatial frequency information content of a scene. The image contaminated by haze is decomposed into different spatial layers with wavelet transforms. Although haze is distributed in the lower frequency layer, this layer may also contain a component of land cover that is spatially and temporally relatively stable. A haze-free reference image of the same area is used to characterise land cover. The component of the characterised land cover is then subtracted wavelet analysis. The residual wavelet coefficients are used to construct a spatially varying mask for subsequent haze detection and removal. After smoothing, the mask is subtracted from the contaminated image to obtain a corrected image with haze-off characteristics. Both visual inspection and statistical accuracy assessment show that the haze calibration is valid and robust.

Introduction

All solar radiation used in satellite remote sensing must pass through the earth's atmosphere. During propagation, this radiation interacts with the atmosphere, generating a variety effects upon the resulting satellite image that must subsequently be accounted for through atmospheric corrections (Teillet, 1997; Cihlar et al., 2000; Du and Gower, 2000). Some atmospheric effects, such as cloud, block almost all radiation in the visible and infrared spectral regions. Others partly obscure the ground-reflected radiation leaving an underlying ground information component in contaminated form. 'Haze' is an example of this latter effect. Haze is a commonly used term in image analysis, referring

to a set of atmospheric effects that reduce image contrast. In general, the impact of haze is evident when viewing images in blue or green parts of the electromagnetic spectrum. At those wavelengths, it is generally an additive radiometric effect and varies spatially, with the resulting satellite image typically exhibiting the underlying ground cover in a diffused pattern. It is imperative that haze be removed prior to scene analysis.

Several different atmospheric scattering or "haze" detection and removal techniques have been reported in the literature. They include simple dark-object subtraction (Vincent, 1973; Chavez, 1988), image-based dark target approaches (Teillet and Fedosejevs,1995), complex atmospheric radiative transfer (RT) modelling (Forster 1984; Spanner et al., 1990; Tanre et al., 1990; Richter, 1990, 1996a), and corrections using *(a)* multi-temporal or multi-channel images (Caselles and Garcia 1989; Hall et al., 1991; Lavreau 1991), *(b)* in situ ground data (Ahern et al., 1977; Otterman and Robinove, 1981) or *(c)* nominally invariant targets (Richter, 1996b).

A major disadvantage of atmospheric RT models is that they require coincident auxiliary information, such as path radiance and/or atmospheric transmission determined at several locations within the image coverage during the satellite overpass. While the use of in situ information might be the most accurate in terms of correcting for atmospheric haze effects, most users must work with remotely sensed data that have already been collected and therefore do not have access to such information. In particular, extensive and potentially very valuable Landsat data have been collected over the last 30 years, in virtually all cases without accompanying information on atmospheric transmittance.

Some techniques use within-scene reference targets. In particular, the simple dark-object subtraction mentioned above is robust requires only information contained in the image data. However, as it is usually implemented, this method can provide only point estimates and its use usually assumes a constant haze value throughout the entire image. It also ignores multiplicative effects, and therefore is of limited use in modelling spatially varying haze over larger scenes.

The present paper focuses on the spatial information content of high-resolution satellite images using wavelet transform analysis techniques. It takes advantage of haze distribution typically being distributed with lower spatial frequency. Although the distribution of land cover also contains some components of low frequency, the latter is comparatively stable in the temporal sense and tends to exhibit distinct texture. If the land cover spatial component can be modelled and removed from the overall low frequency content of an image, the remaining haze contribution can be subtracted from the image to obtain an estimated haze-free rendition. An important potential advantage of this method is its ability to account for complex spatial variation of haze within a scene, thus allowing use of algorithms that depend on image texture or radiometry. Experimental results are presented for the case of a contaminated Landsat Multiple Spectral Scanner (MSS) sub-scene (path 24 row 29) acquired in 1991. This image has been calibrated using wavelet analysis, and corrected with the aid of a haze free reference image from 1986. This scene pair is part of North American Landscape Characterization (NALC) data set (Lunetta, et al, 1998).

Haze and high resolution satellite image

Haze is mainly generated by atmospheric scattering, which is commonly modelled using *Mie* theory. This type of scattering is caused by larger particles present in the atmosphere, including dust, smoke, pollen and water droplets. *Mie* scattering is selective and its effects are wavelength dependent. Under some environmental conditions, more particles occur in the atmosphere, resulting in visually detectable haze, especially at the shorter wavelengths. The spatial distribution of the particles depends on weather conditions (wind, water vapour content, etc.) and the location of dust sources. In a hazy image, a fuzzy outline of land cover usually remains. Because haze propagates through atmospheric disturbances such as wind and convection, the spatial variation of its distribution will be slower (on the scale of kilometers) than for land cover which changes at higher frequencies. Therefore, it can be assumed that in the case of a hazy image the low spatial frequency component is dominated by haze, while the high frequency components reflect the effect of land cover. This spatial scale segregation will be most acute in the case of satellite images with a spatial resolution of less than 100 m, e.g. the Landsat, SPOT and IRS sensor payloads. Finally, typical haze contamination will be most pronounced in the visible bands, and is weaker or visually undetectable in the near- or shortwave- infrared parts of the spectrum.

Because of the frequency dependence of haze effects, wavelet analysis represents a potentially powerful approach. The critical problems in wavelet-based haze correction are the decomposition of the satellite image into different frequency layers and the extraction

of the low frequency component caused by haze. Fortunately, a new and solid mathematical tool, the wavelet transform, can be used for this decomposition task.

Wavelets

Wavelets were developed in signal processing theory to help model temporal signal variability. Wavelet decomposition represents the details of a signal as an alternative manner to convenient temporal and Fourier descriptions. Wavelets can be described for two-dimensional signals, of which satellite images are a special case.

The wavelet approach to signal representation is based on the characteristics of a signal at different scales or, in the case of image, spatial resolutions. At a particular resolution, the signal is approximated by a sum of scaling functions. The difference between the resolutions (termed the detail at the finer resolution) can be expressed by the sum of wavelet functions. For certain scaling and wavelet functions, this hierarchical or multi-resolution representation can be constructed using scaled versions of the same functions at each resolution (Horgan, 1998).

For the one-dimensional case, assume $\{V_j\}_{j\in z}$ is a multi-resolution analysis, $\Phi(x)$ is a scale function, or associated function, and $\Psi(x)$ is a wavelet function. Some properties of $\Psi(x)$ and $\Phi(x)$ are as follows.

The integral of $\Psi(x)$ is zero, ($\int \psi(x)dx = 0$), and $\Psi(x)$ is used to define the details (higher frequencies). The integral of $\Phi(x)$ is 1, ($\int \Phi(x)dx = 1$), and $\Phi(x)$ is used to define the

approximations (lower frequencies). A set of wavelet basis functions, $\{\Psi_{a,b}(x)\}$, can be generated by translating and scaling the basic wavelet, $\Psi(x)$, as

$$\psi_{a,b}(x) = \frac{1}{\sqrt{a}}\psi(\frac{x-b}{a}) \tag{1}$$

where $a>0$ and both a and b are real numbers. The variable a reflects the scale (width) of a particular basis function, while b specifies its translated position along the x-axis.

For the two dimensional case, the discrete wavelet transform, based a tensor products, the two-dimension orthonormal wavelet bases and the multi-resolution orthonormal wavelet decomposition of a digital image $\{C^0_{n,m}\}_{n,m\in z}$ can be formulated. If the total number of decomposition levels is N, the formulae of decomposition of level k are

$$\begin{aligned} C^k_{n,m} &= \sum_{j,l\in Z} \overline{h}_{j-2n}\overline{h}_{l-2m}C^{k-1}_{j,l}, \qquad d^{k2}_{n,m} = \sum_{j,l\in Z} \overline{g}_{j-2n}\overline{h}_{l-2m}C^{k-1}_{j,l}, \\ d^{k1}_{n,m} &= \sum_{j,l\in Z} \overline{h}_{j-2n}\overline{g}_{l-2m}C^{k-1}_{j,l}, \qquad d^{k3}_{n,m} = \sum_{j,l\in Z} \overline{g}_{j-2n}\overline{g}_{l-2m}C^{k-1}_{j,l}. \\ & k = 1,2,.....,N \end{aligned} \tag{2}$$

where $\{h_k\}_{k\in z}$ are orthonormal wavelet filter coefficients $(g_k = (-1)^{k-1}\overline{h}_{1-k})$, and $\{d^{k1}_{m,m}\}$ is the horizontal edge of k level, $\{d^{k2}_{n,m}\}$ the vertical edge, $\{d^{k3}_{n,m}\}$ the diagonal edge, and $\{C^k_{n,m}\}$ the low frequencies.

Figure 1 represents an example of orthonormal wavelet decomposition of an image with four levels. By the wavelet transform, an image can be decomposed into a multi-resolution frame in which every portion has distinct frequency and spatial properties. These properties provide a good base for the analysis, classification and recognition of the image.

Unlike conventional techniques, such as Fourier transform, wavelet decomposition produces a family of hierarchically organized decompositions. The selection of a suitable level of the hierarchy for an application such as haze characterization will depend on the image and human expertise. There are different types of wavelet families whose qualities vary according to several criteria. The selection of a wavelet family for image decomposition will hinge on the properties of the wavelet family and the characteristics of image. We have selected the Daubechies wavelet family (*db*N), a commonly used family of continuous scaling functions and wavelets (Daubechies, 1988). The *db*N includes Haar wavelet, *db*1, the simplest wavelet imaginable and certainly one of the first studied. For *db*N, the support length of Ψ and Φ is *2N-1,* where *N* is the number of vanishing moments of Ψ. Most *db*N are not symmetrical and for some, the asymmetry is very pronounced. The regularity increases with the order. Figure 2 illustrates the different order of wavelet function *db*N in one-dimension.

Wavelet decomposition of an image for the detection and removal of haze

Two co-registered MSS images (path 24 row 29, acquisition dates, Aug. 16 1986 (MSS-86), Aug. 14 1991 (MSS-91)) were used in this study. They constitute part of the *North*

American Landscape Characterization (NALC) data set (Lunetta, et al, 1998). The 1991 image (A) is contaminated by haze (Figure 3a), while the 1986 image (B) is visually much clearer and appears to be haze-free (Figure 3b). We assumed that the 1986 image is haze-free for the purposes of this paper. Two co-registered sub-scenes (2048x2048 pixels) were selected for the study; for convenience, these will be referenced to as image A (1991) and B (1986), respectively. The image dimensions in both pixel and line was selected as powers of two because the recursive nature of wavelet algorithms works best with power-of-two sizes. (If the dimension of an image is not a power of two, its size can be expanded to the next highest power of two through zero-fill padding. After the calculation or processing, the extra space can be removed.) It should be noted that all images and computations are based on the recorded digital numbers.

The various orders of Daubechies wavelet have different properties, including regularity and asymmetry (Daubechies, 1992). In the decomposition of the images for this paper, the properties of the different order of Daubechies wavelet would not be the most important factor as the level of decomposition. Therefore, we chose the *db*4, which has proper length of filter and results in a reasonable haze distribution visually. Wavelet transforms also produce some border distortion during the decomposition of the image, thereby contaminating a narrow strip along the edge of the entire image. The affected width of the strip depends on the level of decomposition. Generally, the higher level of decomposition, the wider range that is affected. However, the border distortion can also be eliminated by extending the size of image with different methods (Cohen, et al. 1993).

Since in this paper we focus on the haze detection, the border distortion will not be discussed in detail.

The level of decomposition for wavelet analysis determines what spatial scale of land cover should be considered relatively stable, higher levels of decomposition being associated with larger spatial scales. If the level of decomposition is too low (i.e. higher spatial frequency level), finer land cover detail will be lost after the haze-off correction. The *db*4 level 5 has been selected as a compromise. In the case of level 4, some land cover detail is lost in the haze-off correction, based on visual inspection, while level 6 is too coarse to provide a proper rendition of the complexities of the haze distribution that can be perceived in Figure 3a.

In applying the procedure, the image A (MSS-91, Band 1) has been decomposed with *db*4 to level 5. When this approximation is reconstructed with the scaling component of level 5, only the lower frequency layer of the image is left and the higher frequency distribution is filtered out (Figure 3d). Obviously, this distribution includes the spatial lower frequency characteristics of both land cover and haze.

We assume that the spatial lower frequency characteristics of the land cover are relatively stable over time. If a reference haze-free image is available, the distribution of its land cover characteristics can be obtained by the same processing. We chose image B (MSS-86, band 1) as the reference image. Figure 3e shows the reconstructed approximation of image B with the scaling component of *db*4 level 5. To extract the land cover lower

frequency characteristics from image A, we processed the scaling components of image A with that of image B to get the approximation components of haze, cA_h:

$$cA_h = \begin{cases} cA - cB & if \quad cA \geq cB \\ 0 & if \quad cA < cB \end{cases} \qquad (3)$$

where, cA is the level 5 approximation coefficient matrix of image A, cB is that of image B, and cA_h is that of haze in image A. Because of residual errors in the geometric registration, some noise occurs after the processing of the haze approximation. Therefore, cA_h is smoothed using (3x3) median filter. Then the approximation of haze is reconstructed with cA_h (Figure 3f).

When the reconstructed haze is subtracted from the hazy image A, the final haze-free estimation is achieved (Figure 3c). The same wavelet analysis is applied to band 2 of the image, with corresponding results shown in Figure 4 a, b, c, d, e and f respectively.

MSS band 3 is a near-infrared channel. A systematic pattern of haze cannot be discerned in its image (Figure 5a), which suggests that the scattering generated by particles in the atmosphere was very weak in the near infrared. The images A and B are visually quite similar in band 3 (Figure 5a, b), which supports the above conclusion. In this case, we ignore the potential effect of haze in the final colour composite reconstruction (Figure 6c).

Visually comparing with original image A (Figure 6a) and haze free image B (Figure 6b) suggests that most haze has been successfully removed. The details of the image are

preserved, however the accuracy of correction is difficult to assess by visual inspection alone.

An analysis of scatter-grams provides further insight into the effect of haze. The relations of band 1 vs. band 3 are shown in Figure 7 a, b, c, and band 2 vs. band 3 in Figure 7 d, e, f for the hazy 1991 image, the 1986 image and the haze corrected 1991 image, respectively. After the correction, although the inter-band relations are changed, which is, however, not enough to explain the substantial visual difference between the hazy and haze-off images. The radiance value (RAD_i) is made up of multiplicative and additive terms. Some of the major contributors to the multiplicative term include the reflectance of the target at pixels (x, y) in band i [$R_i(x, y)$], the slope conditions at pixel (x, y) , the sun zenith angle during data collection , and the atmospheric scattering and absorption characteristics in band i at the time the image is recorded (τ_i). The main contribution to the additive term is due to the path radiance, which is included in the haze term [$haze_i$ (x,y)] in this paper. These factors can be used to obtain a general approximate representation of the radiance parameter [RAD_i (x, y)] in equation (4) as follows:

$$RAD_i(x, y) = R_i(x, y) \times T_i(x, y) + haze_i(x, y) \qquad (4)$$

where $T_i(x,y)$ includes all multiplicative terms. Even if $T_i(x,y)$ were known, R_i (x,y) would be different at the different locations due to spatially varying land cover. If $haze_i(x, y)$ is much less than R_i (x, y), the scatter-plots of haze vs. haze-off will not exhibit a pronounced difference.

To confirm this assumption, we have calculated the average gray levels of each band for all images (Table 1). From Table 1, the mean value of haze is only 15.9% of the total gray level in band 1 and 17.9% in band 2. Therefore, we should not expect the scatter plots to be substantially different. It can also be seen that the mean values of band 3 of image A and B are quite similar, which indicates that band 3 does not need correction. When haze is removed from image A, the mean values in band 1 and 2 of the corrected images are very close to those of the haze-free image B (Table 1). Figure 8 shows the scatter-plot between band 1 and band 2 of haze distribution subtracted from image (A). The haze in band 1 is about 10% higher than band 2 with a high agreement regarding the spatial distribution (correlation coefficient 0.91). Therefore, we conclude that the corrected results for the two bands are consistent and reasonable.

For definitive validation, the simultaneous ground and atmospheric measurements remain the optimum choice but this option is not available for our data set. As an alternative, to estimate the accuracy of the haze removal, we have selected some specific points, which locate in temporally relatively stable urban areas (Figure 9). This type of target has been recommended as generally invariant for change detection studies (i.e. Hall, et al., 1991; Schott, et al., 1988). To avoid the effects of mis-registration, we chose to average the gray levels of 10x10 pixel windows. The differences between haze-off and haze-free means are less than 1 gray level in both bands 1 and 2 (Table 2).

Discussion and conclusions

Our proposed algorithm of the haze detection and removal with wavelet analysis (HAWAT), appears to effectively detect and remove haze over land targets. Although a low-haze or haze-free satellite image is needed as the reference (usually available in existing archives), the technique does not require coincident in situ measurements. If the low frequency distribution of land cover does not change substantially in the area of interest, even a mosaic image of the same area could be used as the reference as long as it is composed of clear scenes.

To extract the haze component from an image with wavelet analysis, two decisions must be made, (a) the selection of the appropriate wavelet family and (b) the determination of the order of wavelet and the level of decomposition. The selection of a wavelet family is an involved mathematical problem, which is not the focus of this paper. We selected the Daubechies wavelet family (*db*N) because it produced a visually reasonable and flexible result and is commonly use for the decomposition of images.

The order of the wavelet transform determines the length of the filter. Generally, the higher order of wavelet transform, the greater than level of detail that is characterized. But instability may occur when the order of *db*N is too high. In our experiment, the result from the order 4 of the Daubechies wavelet was the best based on the visual inspection, so *db*4 was selected for this study.

The level of decomposition is very important to the final result. For example, if we chose the 0 level of decomposition, after the difference between image A and B is subtracted from image A,

image A' = image B (5)

where image A' is the estimated corrected image A. In this case, the difference between A and B in land cover would be removed along with the haze. This is unacceptable for areas with dynamic high frequency information content such as agricultural fields that exhibit significant seasonal variability. On the other hand, if level 10 were selected, which is the highest level for a 2048X2048 image , then the haze distribution would be constant for the entire image.

image A' = image B + constant (6)

All detail of the differences between image A and B would be preserved, with only the average value of the haze is removed. This is similar to conventional dark-object subtraction. It is easy to understand that the level of decomposition determines the balance between haze removal and the preservation of spatial detail. In this paper, the level 4, 5 and 6 were tested with a final selection of level 5 based on visual inspection.

Finally, the higher the level of decomposition, the greater border distortion. This issue will be dealt with in greater detail in a subsequent publication.

The key conclusions of our HAWAT methodology are summarized below:

1. With the decomposition of an image using a wavelet transform, the spatially varying haze can be detected and removed. This technique represents a substantial improvement over dark-object subtraction and other methods, which in most implementations assume spatial invariance of haze.
2. Processing with HAWAT requires only information contained in image-base information, so it is practical and easy to use.
3. By its nature, our algorithm provides a correction procedure in the relative, not the absolute sense, which aims to remove the atmospheric effects in contaminated images relative to a reference image. Therefore, the average gray level values of the hazy image after correction should be similar to the reference image in temporally stable areas. This provides a statistical indicator of quality.
4. The haze distributions of different bands can be subsequently combined to model and infer atmospheric parameters. This problem is currently under study.

The primary drawback of the HAWAT algorithm in its present form is the reliance on operator's expertise in selecting of the decomposition level. Therefore, the development of automated wavelet analysis for haze detection and removal is being considered as well as a more robust methodology which does not require a reference image.

Acknowledgements

The MSS images of this paper are supplied by U.S Environmental Protection Agency, National Exposure Research Laboratory, Environmental Sciences Division. The authors would like to thank Dr. Phil. M. Teillet for his helpful suggestions and advice.

References

Ahern,F.J., Brown,R.J., Cihlar,J., Gauther, R..P., Murphy,J., Neville, R.A., and P.M. Teillet. (1987), Radiometric correction of visible and infrared remote sensing data at the Canada Centre for Remote Sensing. International Journal of Remote Sensing. 8:1349-1376.

Anthis,A.I. and Cracknell, A.P. (1999), Use of satellite images for fog detection (AVHRR) and forecast of fog dissipation (METEOSAT) over lowland Thessalia, Hellas. International Journal of Remote Sensing. 20(6): No.6, 1107-1124.

Caselles, V. and M.J. Lopez Garcia (1989), An alternative simple approach to estimate atmospheric correction in multitemporal studies. International Journal of Remote Sensing. 10:1127-1134.

Chavez, P.S., Jr. (1988), An improved dark-object subtraction technique for atmospheric scattering correction of multispectral data. Remote Sensing of Environment. 24: 459-479.

Cihlar, J., Du, Y. and Latifovic, R. (2001), Land cover dependence in the detection of contaminated pixels in satellite optical data. IEEE Transactions on Geoscience and Remote Sensing. (in review)

Cohen,A., Daubechies, I., Jawerth, B. and Vial, P. (1993), Multiresolution analysis, wavelets and fast wavelet transform on an interval, CRAS Paris, Series A, 417-421.

Daubechies, I.(1988), Orthonormal bases of compactly supported wavelets. Communications on Pure and Applied Mathematics. 41:909-996.

Daubechies, I.(1992), Ten lectures on wavelets, SIAM, PP: 115, 132, 194, 242.

Du,Y. and Gower, J.F.R. (2000), Cloud detection and thin cloud calibration in NOAA AVHRR images with fuzzy logic. Canadian Journal of Remote Sensing. 26(1): 54-63.

Forster, B.C. (1984), Derivation of atmospheric correction procedures for Landsat MSS with particular reference to urban data. International Journal of Remote Sensing. 5(5): 799-817.

Hall, F.G., Strebel, D.E., Nickeson, J.E. and S.J.Goetz (1991), Radiometric rectification: Towards a common radiometric response among multidate, multisensor images. Remote Sensing of Environment. 35:11-27.

Horgan, G.W. (1998), Wavelets for SAR image smooth. Photogrammetric Engineering & Remote Sensing. 64(12): 1171-1177.

Lavreau, J. (1991), De-haze Landsat Thematic Mapper images. Photogrammetric Engineering and Remote Sensing. 57:1297-1302.

Lunetta, R.S., Lyon, J.G., Guindon,B. and Elvidge, C.D. (1998), North American landscape characterization dataset development and data fusion issues. Photogrammetric Engineering and Remote Sensing, 64(8) 821-829.

Ottermen, J., and Robinove, C. J. (1981), Effects of the atmosphere on the detection of surface changes from Landsat Multispectral Scanner data. International Journal of Remote Sensing. 2 (4): 351-360.

Richter, R. (1990), A fast atmospheric correction algorithm applied to Landsat TM images. International Journal of Remote Sensing. 11(1): 159-166.

Richter R. (1996a), Atmospheric correction of satellite data with haze removal including a haze/clear transition region. Computers & Geosciences. 22(6): 675-681.

Richter, R. (1996b), A spatially adaptive fast atmospheric correction algorithm. International Journal of Remote Sensing. 17(6): 1201-1214.

Schott, J.R., Salvaggio,C. and Volchok,W.J.(1988), Radiometric scene normalizaton using pseudoinvariant features, Remote Sensing of Environment. 26,1-16.

Spanner, M.A., Pierce, L.L., Peterson, D.L., and S.W. Running (1990), Remote Sensing of temperate coniferous forest leaf area index: the influence of canopy closure, understory vegetation and background reflectance. International Jounal of Remote Sensing. 11 (6): 1469-1476.

Stephane G. Mallat (1989), Multifrequency channel decompositions of images and wavelet models. IEEE Transactions on Acoustics, Speech, and Signal Processing. 37(12): 2091-2110.

Tanre, D., Deroo, C., Duhaut, M., Morcrette, J.J., Perbos, J., and P.Y. Deschamps (1990), Description of a computer code to simulate the satellite signal in the solar spectrum: the 5S code. International Journal of Remote Sensing. 11 (2): 659-668.

Teillet, P.M. and Fedosejevs, G. (1995), On the dark target approach to atmospheric correction of remotely sensed data. Canadian Journal of Remote Sensing. 21(.4): 374-387.

Teillet, P.M. (1997), A status overview of earth observation calibration/validation for terrestrial applications. Canadian Journal of Remote Sensing. .23(.4): 291-298.

Vincent, R. K. (1973), An ERTS Multispectral scanner experiment for mapping iron compounds. In proceedings of the Eighth International Symposium on Remote Sensing of Environment, Ann Arbor, Michigan. pp1239-1247.

Zhu, C. Q. and Yang, X. M. (1998), Study of remote sensing image texture analysis and classification using wavelet. International Journal of Remote Sensing. 19(16): 3197-3203.

LIST OF TABLES:

LIST OF FIGURES:

Figure 4. The haze detection and removal with wavelet analysis in band 2 (in gray levels). 4a) Original hazy image of band 2, 1991; 4b) Haze free image of band 2, 1986; 4c) Corrected image haze off with wavelet analysis, 1991; 4d) Approximation of hazy image,1991, with db4, level 5; 4e) Approximation of haze free image with db4, level 5; 4f) Calculated haze distribution of original image.

Figure 5. Image 1991 and image 1986 in band 3(in gray levels). 5a) Original hazy image of band 3, 1991; 5b) Original haze free image of band 3, 1986.

Figure 6. Color composition images, Band 1 = blue, Band 2 = red, band 3 = green (in gray levels). 6a) Original hazy MSS image, 1991; 6b) Haze free MSS image, 1986; 6c) Corrected haze off MSS, 1991.

Figure 7. Scatter-plots (in gray levels). 7a) Original hazy image (band1 and band 3), 1991; 7b) Haze free image (band 1 and band 3), 1986; 7c) Corrected image with haze off (band1 and band3); 7d) Original hazy image (band2 and band 3), 1991; 7e) Haze free image (band 2 and band 3), 1986; 7f) Corrected image with haze off (band2 and band3).

Figure 8. Scatter-plot between band 1 and band 2 of haze distributions, 1991 (in gray levels).

Figure 9. The location of check points in the urban areas.

Haze Detection and Removal in High Resolution Satellite Image with Wavelet Analysis

Yong Du☼, Bert Guindon† and Josef Cihlar†

☼ Intermap Technologies Inc., Ottawa, ON, K2E 1A2,† Canada Centre for Remote Sensing, Ottawa, ON, K1A 0Y7

IEEE TGARS, Oct., 2000

A procedure for haze detection and removal from high-resolution satellite image using wavelet analysis (HAWAT) is developed. In HAWAT, the image contaminated by haze is decomposed into different 'spatial layers' using a wavelet transform. Haze is contained in the lower frequency layer, but this layer may also have a component of land cover that is spatially and temporally relatively stable. A haze-free reference image of the same area is used to characterize land cover and to remove its effect from the analysis. The residual wavelet coefficients are used to construct a spatially varying mask for subsequent haze detection and removal. After smoothing, the mask is subtracted from the contaminated image to obtain a corrected, haze-off image. Both visual inspection and statistical assessment of accuracy show that the haze calibration is valid and robust.

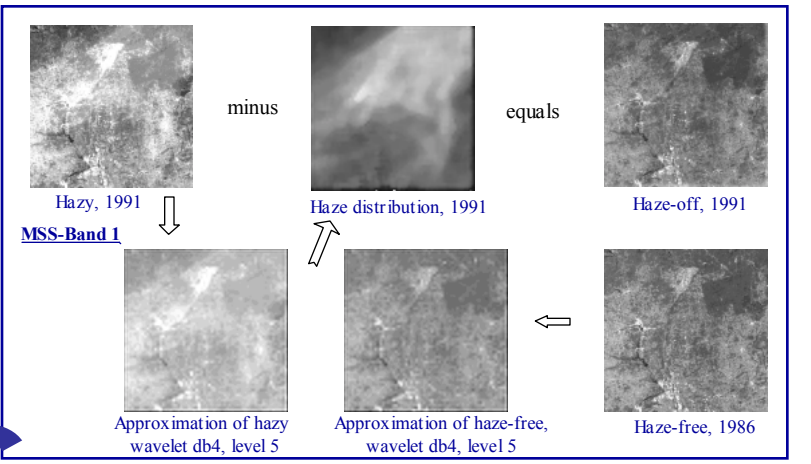

Flowchart of wavelet analysis

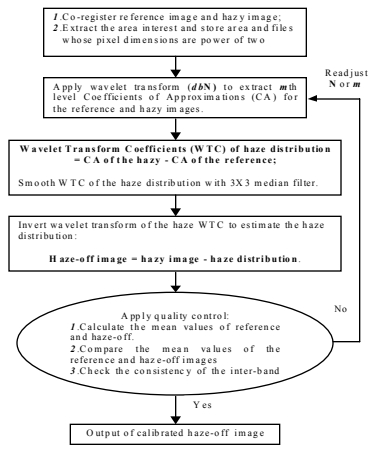

Table 1. Mean values of the different images and haze

	Hazy 91	Haze-free 86	Haze-off 91	Haze 91	Haze %
Band 1	23.3	19.5	19.6	3.7	15.9
Band 2	18.4	15.0	15.0	3.3	17.9
Band 3	53.0	53.4	53.0	0.0	0.0